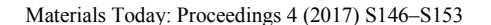


Available online at www.sciencedirect.com

ScienceDirect.





www.materialstoday.com/proceedings

NRW 2016

Macroscopic nanoparticle assemblies: exploring the structural and magnetic properties of large supercrystals*

Genevieve Wilbs^{a,*}, Michael Smik^a, Ulrich Rücker^a, Oleg Petracic^a, Thomas Brückel^a

^aJülich Centre for Neutron Science JCNS and Peter Grünberg Institute PGI, JARA-FIT, Forschungszentrum Jülich GmbH, Germany

Abstract

In the present work we demonstrate, how the self-assembly of nanoparticles provides a simple and straightforward way to fabricate ordered nanocomposites on length scales of up to 300...1000 µm. We realize this by employing a centrifugation assisted sedimentation technique. We start with magnetic iron oxide nanoparticles (NPs) with an average diameter of 15 nm, which are dispersed in toluene. The particles are coated with an organic shell to prevent unordered agglomeration of particles. After centrifugation and subsequent drying large macroscopic assemblies of NPs are obtained. The characterization of the samples using scanning electron microscopy (SEM), x-ray diffraction (XRD) and small angle x-ray scattering (SAXS) reveals that the samples are NP macro-polycrystals. By variation of the fabrication parameters as e.g. centrifugation speed and temperature we obtain a systematic study on how NP ordering, crystallinity and morphology depend on the fabrication parameters. Moreover, the magnetic properties of the NP macro-polycrystals are studied using superconducting quantum interference device (SQUID) magnetometry.

© 2017 Elsevier Ltd. This is an open access article under the CC BY-NC-ND license (http://creativecommons.org/ licenses/by-nc-nd/3.0/).

Selection and Peer-review under responsibility of 7th North Rhine-Westphalian Nano-Conference.

Keywords: nanoparticles; self-assembly; supercrystals; maghemite; SQUID; SAXS; XRD

2214-7853 © 201 7 Elsevier Ltd. This is an open access article under the CC BY-NC-ND license (http://creativecommons.org/ licenses/by-nc-nd/3 0/).

Selection and Peer-review under responsibility of 7th North Rhine-Westphalian Nano-Conference.

^{*} This is an open-access article distributed under the terms of the Creative Commons Attribution-NonCommercial-ShareAlike License, which permits non-commercial use, distribution, and reproduction in any medium, provided the original author and source are credited.

^{*} Corresponding author. Tel.: +49-2461-61-1419; fax: +40-2461-61-2610. E-mail address: g.wilbs@fz-juelich.de

Nomenclature

FWHM Full width half maximum

GALAXI Gallium anode low-angle X-ray instrument MPMS Magnetic property measurement system

NP Nanoparticle

JCNS Jülich Center for Neutron Science SAXS Small angle X-ray scattering SEM Scanning electron microscopy

SQUID Superconducting quantum interference device

XRD X-ray diffraction
ZFC Zero field cooled
FC Field cooled

1. Introduction

Due to their potential use as building blocks for biomedical applications, spintronic devices, refrigeration or high density data storage systems, NPs have recently moved into the focus of intense research activities [1-4]. NPs exhibit novel magnetic, electrical and optical properties that are caused by size effects. These include superparamagnetism, surface plasmons or quantum mechanically discrete energy states [5-7]. For a broad range of materials many characteristics like shape and size have become tunable thanks to rapid developments in chemical synthesis [8-9]. In particular regular arrangements of NPs, similar to atoms in a crystal lattice, i.e. so-called NP supercrystals attract large attention in various scientific fields due to their potential applications as novel type of functional material. Such materials are fabricated by a bottom-up self-assembly approach. It is well known which microscopic phenomena influence the assembling process [10]. However, it still remains challenging to obtain NP arrangements in the desired order because of the large number of interactions contributing and their complex interplay [11]. The ability to tune the ordering by controlling the underlying parameters in order to achieve specific physical or chemical properties appears to be a desirable goal.

In our study we move one step further towards this goal by employing a novel centrifugation assisted sedimentation technique of magnetic iron oxide NPs. We vary several fabrication parameters and characterize the structure obtained and the morphology of the systems. We achieve arrangements with different morphology and degree of order and correlate this to the parameters used.

2. Experimental

2.1 Material

Spherical iron oxide nanoparticles with an average diameter of 15 nm were commercially obtained from Ocean NanoTech, LLC (USA). The NPs were synthesized by thermolysis of an iron precursor. Oleic acid was added as surface ligand to control the particle size during synthesis and to avoid uncontrolled agglomeration. The NPs are initially dispersed in toluene.

2.2. Methods

For the investigation of the NP shape and NP arrangement at the supercrystal surface an SU8000 SEM from Hitachi was employed. Magnetometric measurements were performed using an MPMS SQUID magnetometer from Quantum Design. To determine the specific iron oxide phase and composition, XRD was performed in transmission geometry using a copper X-ray source combined with a curved germanium (111) monochromator crystal and the

Guinier G670 X-ray camera from Huber which utilizes image plate detection. The nanoparticle size, size dispersion and order were identified by small angle X-ray scattering (SAXS) experiments with the Gallium Anode Low-angle X-ray Instrument (GALAXI) at the Jülich Center for Neutron Science (JCNS). It includes a MetalJet X-ray source from Bruker AXS for X-ray generation and a Pilatus 1M detector from Dectris for radiation detection [12].

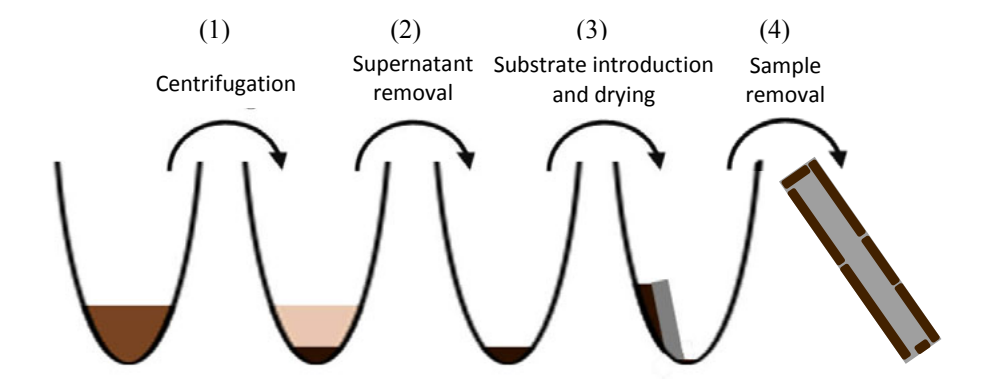


Fig. 1: Schematic representation of the preparation procedure for NP supercrystals employing a centrifugation approach (not to scale). (1) The NP dispersion is placed into a centrifuge. (2) After centrifugation the supernatant is removed and (3) a Silicon substrate introduced. (4) After drying the Silicon substrate with the attached NP supercrystals is removed.

2.3. Supercrystal preparation

The concentration of the NP dispersion was adjusted to 25 mg NP / ml toluene and $50 \,\mu$ l were filled into a conical screw cap polypropylene microcentrifuge sample tube. The sample was then centrifuged for $2 \, h$ at various fixed accelerations and at various but constant temperatures using a Heraeus Fresco $21 \, \text{refrigerated}$ microcentrifuge from Thermo Scientific. The centrifugation leads to forced NP sedimentation. Ca. $30 \, \mu$ l supernatant were subsequently removed using a micropipette and a polished clean $10 \, x \, 2 \, \text{mm}^2$ silicon substrate was carefully pushed into the sediment. The sediment still contains significant solvent and moves upwards along the substrate due to capillary forces. At e.g. 17°C most of the solvent evaporates within $24 \, h$, mainly at the substrate edges, leading to an outward flow of the nanoparticles. As a result, supercrystals form at the substrate edges. Figure 1 schematically shows the main steps of the preparation procedure.

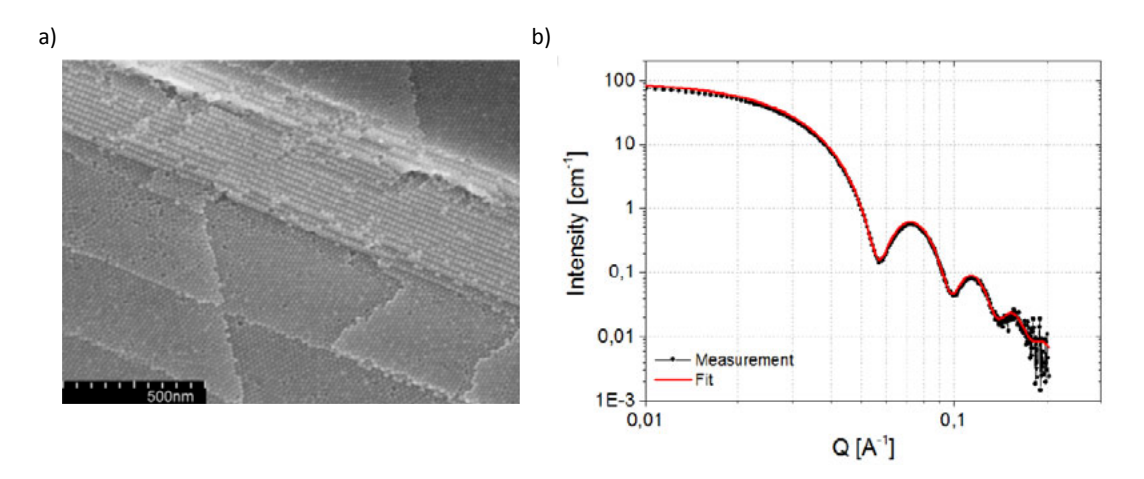


Fig. 2 (a) SEM image of NPs at the supercrystal surface; (b) SAXS measurement of the nanoparticle dispersion at a concentration of 0.8 mg NP/ml toluene (black) and fit to the curve (red).

3. Results and Discussion

3.1. Nanoparticle characteristics

The SEM image shown in figure 2 (a) obtained at the surface of a supercrystal demonstrates the spherical shape of the NPs and can be also employed for a rough size estimate (diameter ca. 15 nm). Moreover, also the NP order can be seen. We find relatively well ordered 'supercrystallites' with an ordered arrangement of more than 100 NPs along one direction. The ordering appears to be either hexagonal closed packed or simple cubic. A more accurate determination of size and ordering is derived from SAXS measurements performed at GALAXI. Using a nanoparticle dispersion at a concentration of 0.8 mg NP / ml toluene the intensity I in dependency of the absolute value of the scattering vector Q was measured (figure 2 (b)). Using the SasView software a sphere-model function was fitted to the data resulting in an average nanoparticle diameter of 15.6 nm and a size dispersion of 13.5 %.

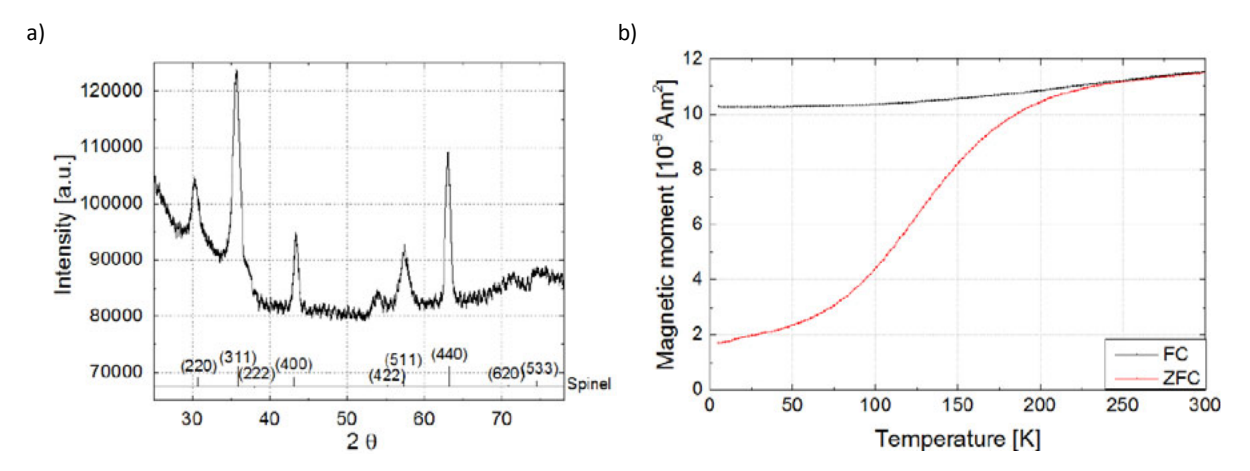


Fig. 3 (a) XRD pattern obtained from dried NPs deposited on a Mylar foil; (b) Magnetometric ZFC (red) and FC (black) curves measured at an applied magnetic field of 50mT.

Figure 3 (a) shows the XRD pattern measured on nanoparticles deposited on a Mylar foil. A fit to the data reveals that the NPs contain a spinel structure that can either correspond to maghemite (γ -Fe₂O₃) or magnetite (Fe₃O₄) [13]. In figure 3 (b) zero-field-cooled (ZFC) and field-cooled (FC) curves of the magnetic moment are depicted. Here a *single* supercrystal was removed from the substrate and mounted for magnetometric measurements. For the ZFC curve the sample was cooled to 10 K in zero field. Subsequently, the magnetic moment was recorded upon warming in a small magnetic field of 5 mT. For the FC curve the magnetic moment was measured while cooling down from room temperature to 5 K at the same applied field of 5 mT. Since no feature at the Verwey transition of magnetite at 120K is found [14], we exclude the presence of magnetite. Therefore, we conclude that the NPs consist of maghemite.

The magnetic properties observed here can be understood in terms of superparamagnetism and dipolar interactions between the particles [15-17]. The nanoparticles are assumed to be in a monodomain state since the critical single domain radius for iron oxide particles is ca. 30 nm. The shapes of the ZFC and FC curves, i.e. the presence of a peak in the ZFC curve (decrease of magnetic moment at elevated temperature not shown) and the splitting of the FC curve close to the peak matches with the usual behavior observed in superparamagnetic NP systems [18-19]. In addition, the FC curve shows a slight decrease with decreasing temperatures, which indicates that significant dipolar interactions are present in the sample. This is expected since the NPs are densely packed in the supercrystals.

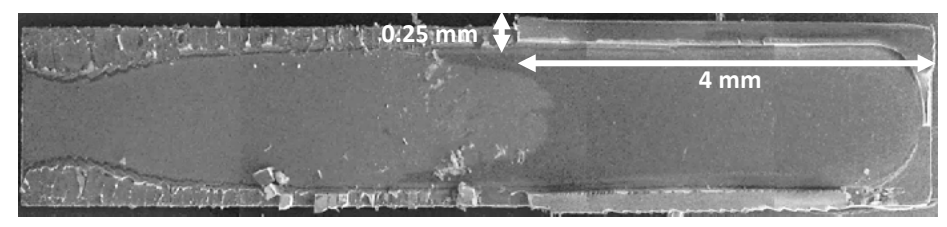


Fig. 4 SEM image of the macrocrystals formed on a 10 x 2 mm² silicon substrate.

3.2. Supercrystal characteristics

For the investigation of the influence of the process parameters 21 samples were prepared at 0° C differing only in the centrifugation acceleration. Accelerations of 1 000 x g, 2 000 x g, ..., 20 000 x g and 21 000 x g were used. To check for the influence of the centrifugation temperature, further 21 samples were prepared at temperatures 10° C, 20° C and 30° C. Figure 4 exemplarily shows one of the resulting samples, where a 0.25×4 mm² supercrystal can be observed in the upper right corner.

3.2.1. Supercrystal morphology

The supercrystals exhibit basically a rectangular shape. However, their number and sizes differ significantly depending on the centrifugation parameters. In order to assess the 'quality' of the supercrystals a phenomenological 'score value' S is introduced. Only if the shorter side of the supercrystal was larger than $100 \mu m$ the supercrystal was counted while the length of the longer side was used to assign it to one of the size categories shown in table 1. Depending on its height and width, every single supercrystal was additionally assigned to one of the shape categories also summarized in table 1. This allows for the determination of the score value for every size category, depending on the amount of supercrystals in each shape category N_A , N_B , N_c . The score value includes a weighting of the categories in the following way:

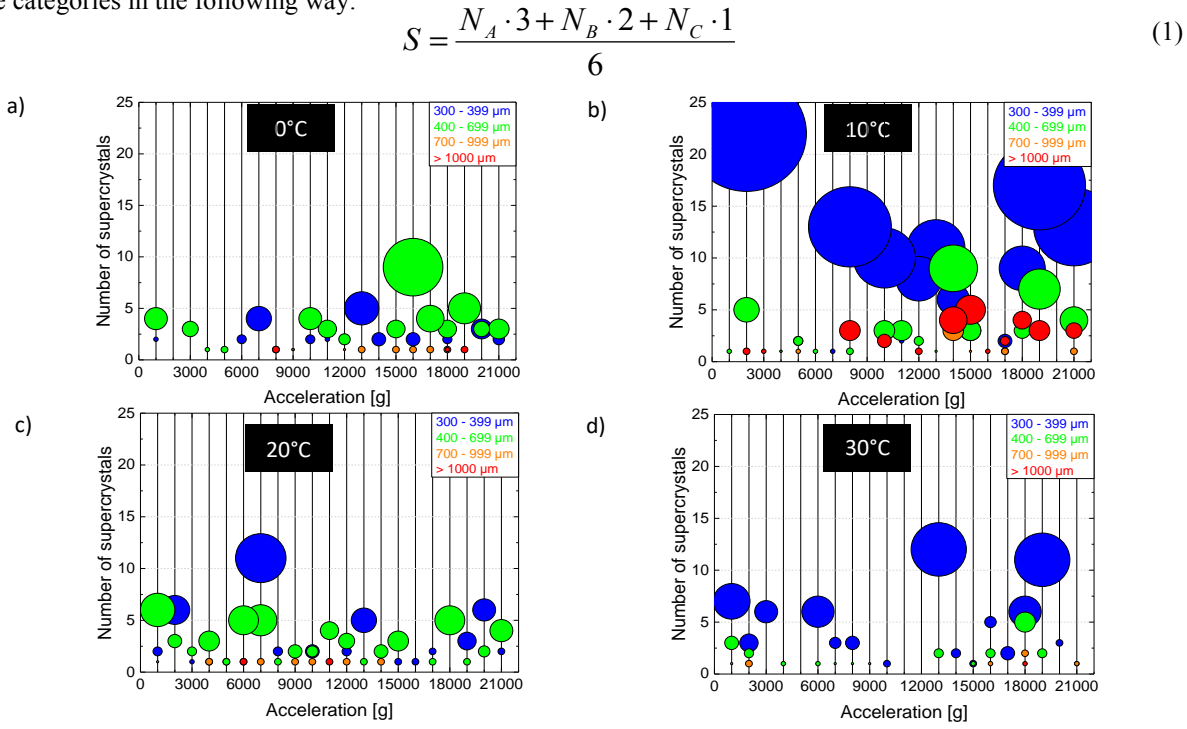


Fig. 5 Number of supercrystals for each sample separated by size category. The x-axis shows at which acceleration the sample was prepared. The diameter of the dots is proportional the score value calculated for every size category separately. The samples were prepared at (a) 0°C, (b) 10°C, (c) 20°C and (d) 30°C, respectively.

Size categories	Shape categories
300 399 μm	A: height > 100 μm, width > 200 μm
$400\dots699~\mu m$	B: height $> 100 \mu m$, width $< 200 \mu m$
$700 \dots 999 \ \mu m$	C: height < 100 µm
> 1000 µm	

Table 1. Summary of size and shape categories.

Figure 5 shows the summarized data for all samples prepared at (a) 0°C, (b) 10°C, (c) 20°C and (d) 30°C. Every acceleration value corresponds to a single sample. The diameter of the dots is proportional to the score value S calculated according to equation (1) and its color corresponds to the size category. The results obtained at 0°C and 20°C are very similar. At 30°C the total amount of supercrystals is significantly lower and most of them are assigned to the smallest size category. The best results were obtained with samples centrifuged at 10°C. At this temperature the highest amount of supercrystals was counted and the longest supercrystals were found. This might be due to the temperature dependent state of the oleic acid coating. Its bulk melting temperature is 16.3°C [20]. Therefore one might assume that also for the oleic acid coating around the NPs the melting temperature will have an effect although no melting-freezing scenario will occur as in bulk. However, the coating will show different 'stiffness' and hence different steric repulsion properties, i.e. supercrystals centrifuged at 0°C and 10°C will experience an overall stiffer behavior. Another factor is the post-centrifugation drying process which occurs at 17°C. One should note that very likely the self-assembly process into the final supercrystal state happens during this drying process, while the centrifugation 'prepares' the system into a dense, gel-type precursor state. This means that the self-assembly process basically occurs during drying.

Consequently, samples centrifuged at 0°C or 10°C will experience simultaneously warming and drying or with other words a softening of the coating and the self-assembly. This will lead to different ordering and morphologies compared to the samples centrifuged at 20°C and 30°C where no warming up occurs.

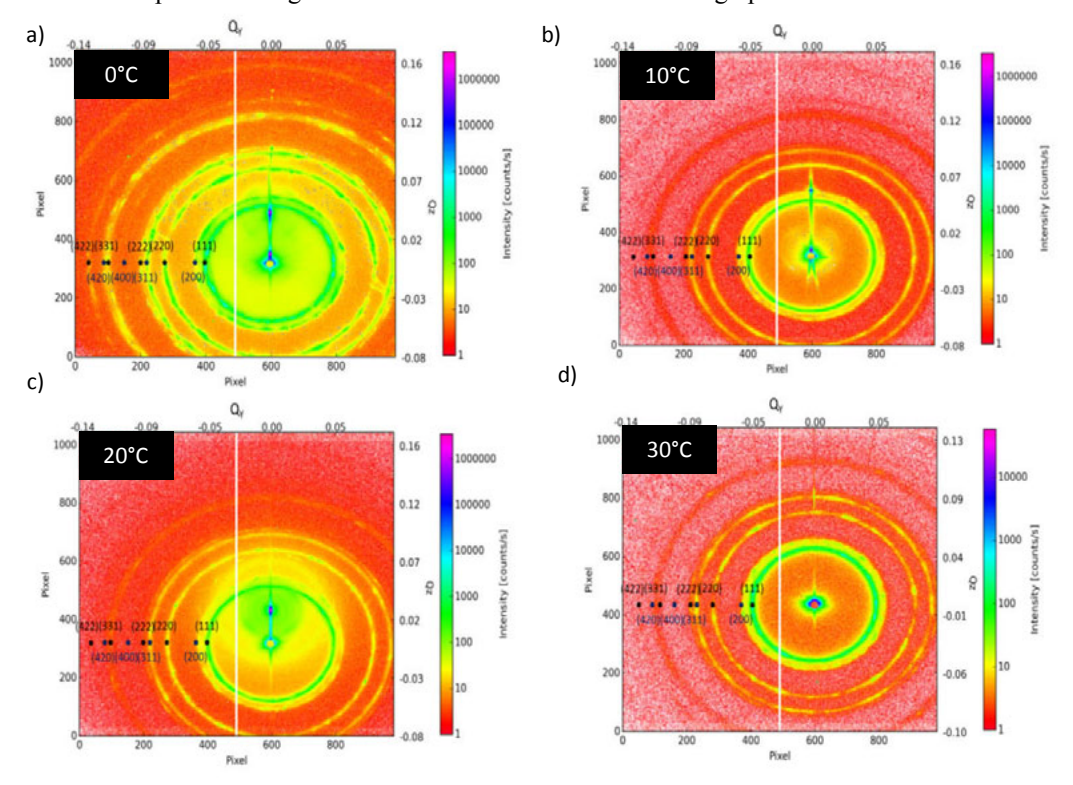


Fig. 6 SAXS patterns measured on single supercrystals that were centrifuged at 21 000 x g. The centrifugation temperature was (a) 0°C, (b) 10°C, (c) 20°C, (d) 30°C.

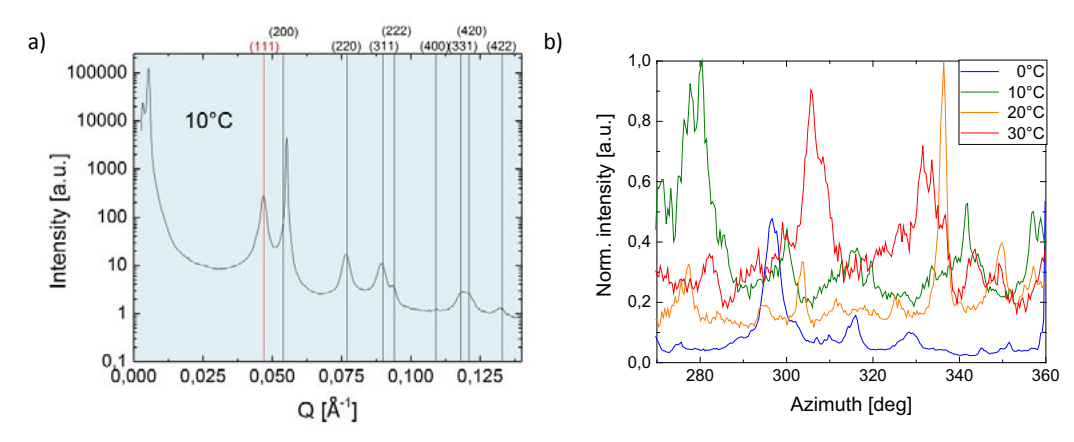


Fig. 7 (a) Radial integrated intensity for the supercrystal obtained after centrifugation at 10°C. The measured (111) peak is marked in red, the calculated positions of further peaks for a FCC lattice are shown in black. (b) Integrated intensities of the fourth quadrant on the (220) powder ring, normalized to 1 as function of the azimuthal angle.

Concerning the centrifugation acceleration no significant influence is observed at 0°C, 20°C and 30°C. At 10°C on the other hand, long supercrystals with a high score value are preferably found from 8 000 x g upwards. This is attributed to the better phase separation at higher accelerations.

3.2.2. Nanoparticle order

Figure 6 shows SAXS patterns of single supercrystals removed from samples centrifuged at 21 000 x g and (a) 0°C, (b) 10°C, (c) 20°C and (d) 30°C. Assuming a cubic Bravais lattice as indicated by the SEM image shown in figure 2 (a), the first ring corresponds to the (111) peak [21]. The corresponding Q value is 0.046±0.001 Å⁻¹ for all four measurements and leads to a lattice constant of 23.9±0.5 nm which fits the determined nanoparticle diameter if a face centered system is assumed. This is confirmed by further peak positions that fit to the allowed peaks for such an arrangement as exemplarily shown in figure 7 (a) for the sample centrifuged at 10°C.

We also find that the intensity distribution on the rings is textured to different extents. Figure 7 (b) shows the radially integrated intensities in the fourth quadrant of the (220) powder ring derived from the SAXS pattern as function of the azimuthal angle as shown in figure 6. While a powder system would show only an isotropic ring, i.e. no azimuthal dependence, a perfect single (super)crystal would display sharp peaks with vanishing intensity in between. Here we find that the supercrystal centrifuged at 20° C exhibits sharp peaks with a small FWHM (e.g. ΔQ =0.00016 nm⁻¹ at 336°) superimposed on a constant powder ring background. Hence, this sample mainly consists of disordered powder and additionally contains a small number of grains with a large coherence length (e.g. 36.5 μ m for ΔQ =0.00016 nm⁻¹) and can therefore be understood as NP macro-polycrystal. The supercrystals centrifuged at 0°C, 10°C and 30°C consist of a textured powder. They contain a larger number of ordered grains which exhibit different orientations leading to broader peaks. Hence, concerning the aim of fabricating supercrystals that contain only one single ordered grain, the best result was obtained at a centrifugation temperature of 20°C.

4. Conclusion

A novel centrifugation assisted self-assembly approach for the preparation of macroscopic supercrystals was introduced. The employed iron oxide nanoparticles were characterized in detail using imaging and scattering techniques. It is demonstrated how the morphology of the supercrystals can be investigated and the nanoparticle order by a small angle scattering technique. The parameters centrifugation temperature and speed significantly influence the supercrystal properties. They can be adjusted to fabricate huge, ordered assemblies.

References

- [1] B. D. Terris, T. Thomson, J. of Phys. D: Appl. Phys. 38 (2005) 12 R199
- [2] A. Karmar, J. of Phys. (2011) 012002
- [3] R. Saidur, S. N. Kazi, M. S. Hossain, M. M. Rahman, H. A. Mohammed, Renew, and Sust. Energy, Rev. 15 (2011) 1 pp. 310-323
- [4] K. P. Ghatak, S. Bhattacharya, D. De, Nanostructure Science and Technology Photoemission from Optoelectronic Materials and their Nanostructures, Springer, 2009
- [5] H. A. Atwater, Sci. Am. 296 (2007) 4 pp. 56-63
- [6] D. J. Norris, A. I. Efros, S. C. Erwin, Science 319 (2008) 5871 pp. 1776-1779
- [7] O. Petracic, Superlattices and Microstructures 47 (2010) 5 pp. 569-578
- [8] S. Sun, Adv. Mater. 18 (2006) pp. 393-403
- [9] S. Bedanta, A. Barman, W. Kleemann, O. Petracic, T. Seki, J. of Nanomat. 952540 (2013)
- [10] K. J. M. Bishop, C. E. Wilmer, S. Soh, B. A. Grzybowski, Small 5 (2009) 1600e1630
- [11] S. Disch, E. Wetterskog, R. P. Hermann, G. Salazar-Alvarez, P. Busch, T. Brückel, L. Bergström, S. Kamali, Nano Lett. 11 (2011) 1651e1656
- [12] E. Kentzinger, M. Krutyeva, U. Rücker, J. of large-scale research facilities 2 (2016) A61
- [13] A. M. Jubb, H. C. Allen, Appl. Mat. & Inter. 2 (2010) 10 pp. 2804-2812
- [14] F. Walz, J. Phys.: Condens. Matter 14 (2002) R285-R340
- [15] W. F. Brown, Phys. Rev. 130 (1963) 1677e1686
- [16] J. J. Dormann, D. Fiorani, E. Tronc, Adv. Chem. Phys. 98 (1997) 283e494
- [17] X. Batlle, A. Labarta, J. Phys. D: Appl. Phys 35 (2002) R15eR42
- [18] L. Néel, Ann. Geophys. 5 (1949) 99e136
- [19] S. Bedanta, O. Petracic, W. Kleemann, Supermagnetism, Handbook of Magnetic Materials Vol 23, Ed. K. J. H. Buschow, Elsevier (2015)
- [20] D.R. Lide, Handbook of Chemistry and Physics, CRC Press 2005
- [21] Online: ResearchGate, Laboratory module 1: indexing x-ray diffraction patterns